Journal of Oceanography, Vol. 61, pp. 141 to 154, 2005

Air-Sea Interactions under the Existence of Opposing Swell

HISASHI MITSUYASU[1]* and YOSHIKAZU YOSHIDA[2]

[1]*Professor Emeritus of Kyushu University*
[2]*Japan Port Consultants, Fukuoka 812-0014, Japan*

(Received 26 February 2004; in revised form 11 May 2004; accepted 17 May 2004)

Data of a comprehensive laboratory study on the coexistent system of wind waves and opposing swell (Mitsuyasu and Yoshida, 1989) have been reanalyzed to clarify the air-sea interaction phenomena under the coexistence of wind waves and swell. It is shown that the magnitude of the decay rate of swell due to an opposing wind is almost the same as that of the growth rate of swell caused by a following wind, as measured by Mitsuyasu and Honda (1982). The decay rate is much smaller than that obtained recently by Peirson *et al*. (2003), but the reason for the disagreement is not clear at present. The effect of an opposing swell on wind waves is very different from that of a following swell; wind waves are intensified by an opposing swell while they are attenuated by a following one. The phenomenon contradicts the model of Phillips and Banner (1974), but the reason for this is not clear at this time. The high-frequency spectrum of wind waves shows a small increase of the spectral density. Wind shear stress increases a little due to the effect of opposing swell. The intensification of wind waves by opposing swell and the small increase of the spectral density in a high-frequency region can be attributed to the increase of wind shear stress. Such organized phenomena lead to the conclusion that the hypothesis of local equilibrium for pure wind waves (Toba, 1972) can also be satisfied for wind waves that coexist with opposing swell. The recent finding of Hanson and Phillips (1999) can be explained by this mechanism.

Keywords:
- Air-sea interactions,
- swell,
- wind waves,
- interaction between wind waves and swell,
- sea surface roughness,
- local equilibrium of winds and wind waves.

1. Introduction

During the past forty year or so, many studies have been conducted on the effect of swell on air-sea interactions (Mitsuyasu, 1966, 1997; Phillips and Banner, 1974; Wright, 1976; Hatori *et al*., 1981; Donelan, 1987, 1999; Dobson *et al*., 1988; Tsuruya, 1988; Masson, 1993; Sakai *et al*., 1994; Hanson and Phillips, 1999; Mitsuyasu and Maeda, 2002). However, the problem is still controversial and consistent results have not yet been obtained (Hanson and Phillips, 1999). Furthermore, many of these studies are concerned with individual phenomena such as attenuation of wind waves by following swell, growth of swell by following wind, and attenuation of swell by opposing wind, but these phenomena are generated simultaneously. For example, when swell enters a wind area the swell is developed or attenuated by the wind, depending on the direction of the wind relative to the propagation direction of the swell. At the same time, the wind wave changes due to the effects of swell; attenuation of wind waves is caused if the following swell is steep. Furthermore, sea surface roughness may be affected by steep swell entering a wind area.

In order to clarify such complicated phenomena, about 15 years ago we conducted a comprehensive laboratory study on air-sea interactions under the existence of opposing swell (Mitsuyasu and Yoshida, 1989). Unfortunately, however, results of the study were published only in the *Bulletin of the Research Institute for Applied Mechanics of Kyushu University* (in Japanese), although some selected results concerning special phenomena were published in the proceedings of several international symposia and international journals (Mitsuyasu and Yoshida, 1991; Mitsuyasu, 1992, 1997).

Recently, similar studies have been done, independently of our previous study, but these studies have been concerned only with some particular phenomenon (Donelan, 1999; Peirson *et al*., 2003). The present au-

* Corresponding author. E-mail: mituyasu@hf.rim.or.jp
Present address: Fukuoka 811-0212, Japan.

thors have come to the conclusion that the publication of the total results of our previous study for the international community is necessary to present fundamental reference data for similar studies. In the present paper we present the comprehensive results of our previous study, after re-examination of the important results of that study in light of other recent studies.

2. Equipment and Procedures

2.1 Wind-wave flume and measurements

The experiment was carried out in a small wind wave flume 0.8 m high (water depth 0.35 m), 0.6 m wide and with the usual 15 m long test section. The air gap between the still water surface and a transition plate is 5 cm. The arrangement of the equipment is shown schematically in Fig. 1. A flap-type wave generator at the right-hand side of the flume generates swell (monochromatic wave). The swell periods were T = 0.620, 1.024 (sec) and their initial heights were H = 1.3, 2.6 (cm) for the waves of T = 0.620 (sec) and H = 3.0 cm for the wave of T = 1.024 sec. The swell energy was absorbed in a beach installed at the left-hand side of the flume. A centrifugal fan (outside the figure to the left) sends the wind in the opposite direction to the swell. The wind speed is monitored with a Pitot static tube installed 15 cm above the transition plate at the inlet of the flume. The wind speed measured at this point is used as a reference wind speed and is denoted *Ur*. The reference wind speed was changed stepwise as *Ur* (m/s): 5.0, 7.5, 10.0 and 12.5. Wind generates wind waves, which propagate from left to right through the test section of the flume, finally to be absorbed by a wire-mesh filter in front of the wave generator. Swell (mechanically-generated wave) passes through the filter, with small attenuation, since it has a longer period than that of the wind wave. Waves were measured at eight stations (No. 1~No. 8) using resistance type wave gauges installed in the flume at 1 m separations. Waves were recorded with a digital data recorder at a sampling frequency of 200 Hz. The vertical wind profile over the water surface, $U(z)$, was measured with a Pitot static tube at four stations, F1~F4. The experimental conditions are summarized in Table 1.

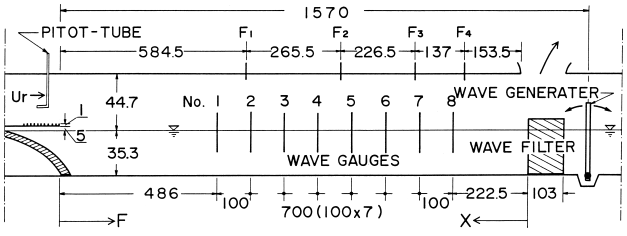

Fig. 1. Schematic diagram of wind wave flume (cm).

Table 1. Experimental condition.

Run No.	*Ur* (m/s)	*T* (sec)	*H* (cm)	λ (cm)	H/λ ($\times 10^2$)	
1–1	5.0					Wind waves
1–2	7.5					
1–3	10.0					
1–4	12.5					
2–1	5.0	1.024	3.0	148	2.03	Wind waves and swell
2–2	7.5	1.024	3.0	148	2.03	
2–3	10.0	1.024	3.0	148	2.03	
2–4	12.5	1.024	3.0	148	2.03	
3–1	5.0	0.64	1.3	63.8	2.04	Wind waves and swell
3–2	7.5	0.64	1.3	63.8	2.04	
3–3	10.0	0.64	1.3	63.8	2.04	
4–1	5.0	0.64	2.6	63.8	4.08	Wind waves and swell
4–2	7.5	0.64	2.6	63.8	4.08	
4–3	10.0	0.64	2.6	63.8	4.08	
5–1	0	1.024	3.0	148	2.03	Swell
5–2	0	0.64	1.3	63.8	2.04	
5–3	0	0.64	2.6	63.8	4.08	

Ur: reference wind speed, *T*: wave period, *H*: initial wave height, λ: wave length, H/λ: initial wave steepness.

2.2 Experimental procedure

The wave measurements were done under the following three different conditions; pure wind waves without swell, wind waves coexisting with opposing swell, and swell without wind. Practical procedures are as follows: wind-generated waves in a steady state were measured first, then swell was generated and sent into a generation area of the wind waves and the coexistent system of wind waves and opposing swell in a steady state was measured. In order to determine the attenuation rate of the swell due to water viscosity, the swell was measured independently without wind action. The attenuation data determined from the latter measurement were used to determine the attenuation rate of swell due to opposing wind by correcting for the effect of water viscosity. Wind profiles were also measured independently of the wave measurements for each water surface condition.

2.3 Analysis of the wave data

The wave data from each run were divided into six samples, each of which contained 4096 digitized data. Power spectra of waves were computed through a FFT method using each 4096-point data set. After taking the sample mean of six spectra, the spectra were smoothed using triangular filters. Numbers of the spectral lines within the filter were adjusted depending on each frequency band, as shown in Table 2.

3. Results

3.1 Wind profiles and water surface roughness

Vertical wind profiles over the water surface, $U(z)$, were measured both for pure wind waves and for the coexistent system of wind waves and opposing swell. Figure 2 shows some examples of wind profiles over pure wind waves, which were measured at a fetch F = 5.845 m.

As shown in Fig. 2 the wind profiles show the well-known logarithmic distribution,

$$U(z) = \frac{u_*}{\kappa} \ln \frac{Z}{Z_0}, \qquad (1)$$

where u_* ($= \sqrt{\tau / \rho_a}$) is the friction velocity of the wind,

Table 2. Spectral filters.

Frequency band (Hz)	Number of the spectral lines
$f \leq 3$	1
$3 < f \leq 10$	11
$10 < f \leq 40$	21
$40 < f \leq 100$	41

τ the wind shear stress, ρ_a the air density, κ the Kármán's constant (≈0.4) and Z_0 the roughness parameter. Figure 3 shows the wind profiles over the water surface where wind waves and opposing swell coexist. For comparison, the wind profiles over pure wind waves without swell shown previously in Fig. 2, are inserted in the figure with broken lines without showing the data points. Figure 3 shows that opposing swell causes a slight change of the wind profile in the direction of increasing friction velocity. The values of u_* and Z_0 were determined by fitting the logarithmic distribution (1) to the measured wind profiles.

Furthermore, we determined the wind speed U_{10} at height Z = 10 m by

$$U_{10} = \frac{u_*}{\kappa} \ln \frac{10}{Z_0}, \qquad (2)$$

and the wind speed U_λ at the height of one wavelength λ for each swell by

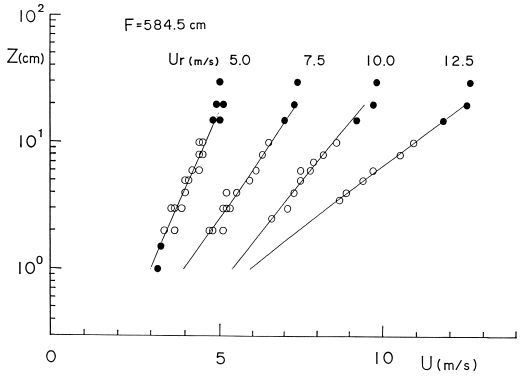

Fig. 2. Wind profiles over pure wind waves.

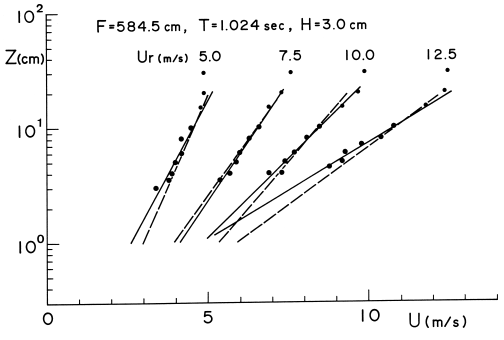

Fig. 3. Comparison of wind profiles over two different wave systems. —: Wind profiles over coexistent system of wind waves and opposing swell. - - -: Wind profiles over pure wind waves.

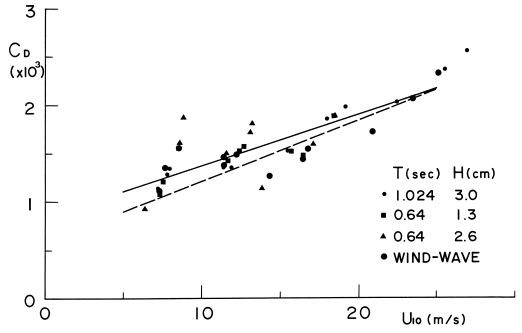

Fig. 4. Plot of the drag coefficient C_D versus wind speed U_{10}. —: Eq. (5), - - -: Eq. (6).

$$U_\lambda = \frac{u_*}{\kappa} \ln \frac{\lambda}{Z_0}. \tag{3}$$

These characteristic wind speeds will be used later in the analysis of wave data.

In order to clarify the change of surface roughness due to opposing swell we determined the drag coefficient C_D by

$$C_D = (u_*/U_{10})^2. \tag{4}$$

Figure 4 shows the relation between the drag coefficient C_D and the wind speed U_{10} . The solid line is a least-square fit to the present data, which is given by

$$C_D = (0.841 + 0.053U_{10}) \times 10^{-3}, \tag{5}$$

and the broken line corresponds to the relation for a pure wind wave surface, which is taken from Mitsuyasu and Kusaba (1984) and is given by

$$C_D = (0.581 + 0.063U_{10}) \times 10^{-3}. \tag{6}$$

Although the data scatter considerably, the following trends can be seen.

1) The drag coefficient increases slightly due to the coexistence of opposing swell.

2) There seems to be a systematic change of C_D due to fetch.

The second statement implies the following property: We can see four clusters of the data in Fig. 4. The clusters of the data correspond to four reference wind speeds, *Ur* (m/s): 5.0, 7.5, 10.0, and 12.5. Although the fetch is not shown in the figure, scatter of the data within each cluster is due to the effect of the fetch. The fetch-dependence of the drag coefficient may be expected, because wind waves develop with fetches and their scales as a surface roughness increase with fetches. Fetch-dependence or wave-dependence of wind shear stress will be discussed later in Subsection 3.3.

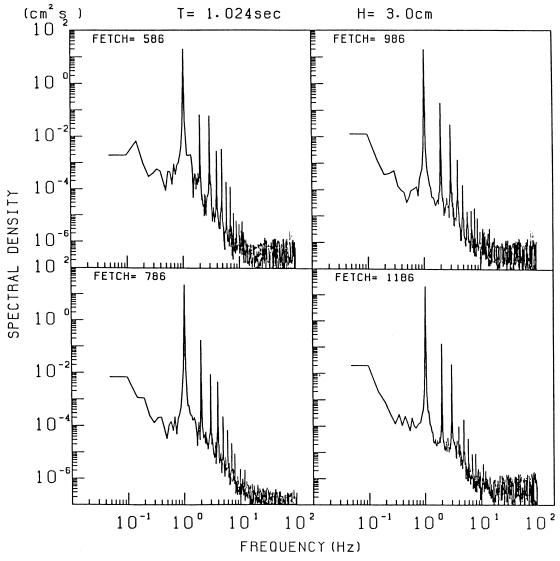

Fig. 5. Spectra of swell without wind action. Stations: No. 2, No. 4, No. 6, No. 8.

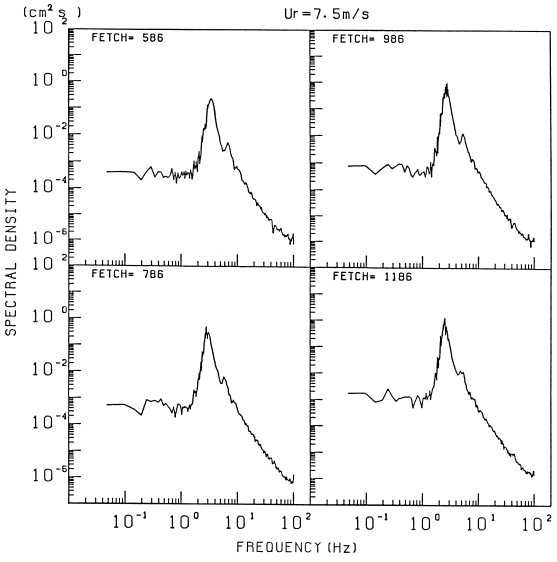

Fig. 6. Spectra of pure wind waves. Stations: No. 2, No. 4, No. 6, No. 8.

3.2 Wave spectra

Figure 5 shows some examples of the spectra of swells (mechanically-generated monochromatic waves) without wind action, which were measured at station Nos. 2, 4, 6 and 8. As usually observed, the spectra show many higher harmonics due to the nonlinearity of water waves. Figure 6 shows the spectra of pure wind waves measured

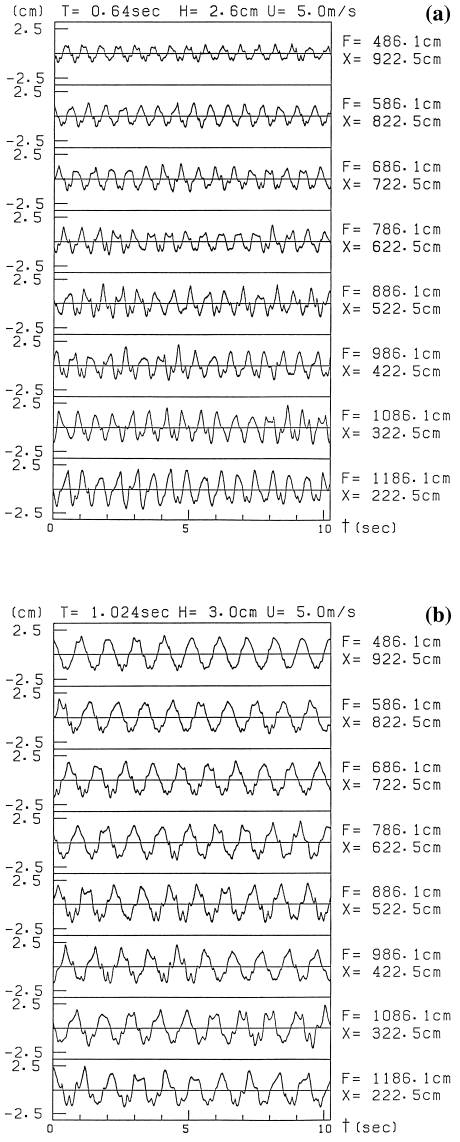

Fig. 7. Sample records of coexistent system of wind waves and swell. (a) Swell: T = 0.64 sec, H = 2.6 cm, Ur = 5.0 m/s. (b) Swell: T = 1.024 sec, H = 3.0 cm, Ur = 5.0 m/s.

at the same stations for a wind speed of Ur = 7.5 m/s. The swell spectra and the pure wind wave spectra were used as reference data for the analysis of the spectral data of the coexistent system of wind waves and opposing swell. Figures 7(a) and (b) show sample records of the coexistent system of wind waves and opposing swell. In these figures, F means the fetch measured from the end of the transition plate and X means the distance measured from the end (left side) of the wave filter. With increasing fetch (from the top to the bottom), the waveform gradually becomes complicated due to the growth of wind waves superimposed on the opposing swell. Note that the swell is propagating in the opposite direction, from the bottom to

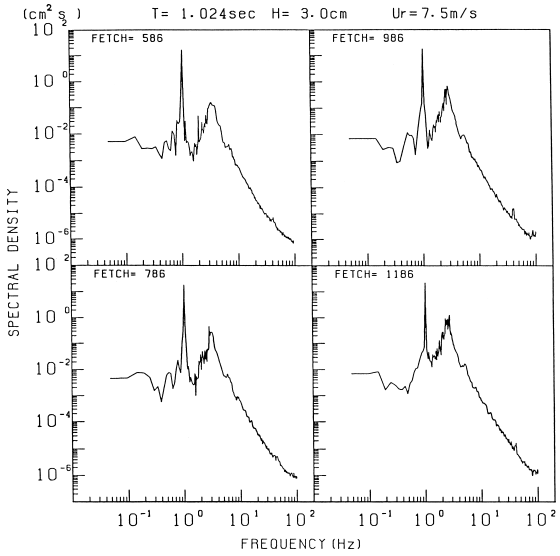

Fig. 8. Spectra of coexistent system of wind waves and swell. Stations: No. 2, No. 4, No. 6, No. 8.

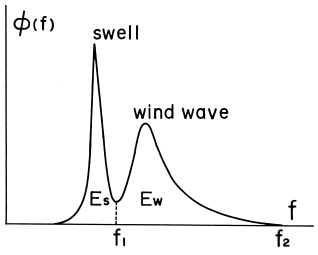

Fig. 9. Diagram of the wave spectrum of coexistent system of wind waves and swell (f_1 = 1.8 Hz, f_2 = 40 Hz).

the top. Therefore we can clearly see the attenuation of the short-period swell (cf. Fig. 7(a)).

Figure 8 shows some examples of the spectra of coexistent system of wind waves and opposing swell. A very sharp peak in the low-frequency region corresponds to the swell spectrum and a secondary peak in the high-frequency region corresponds to the wind wave spectrum. In the present experiment the wind wave spectrum and the swell spectrum have different frequency regions, as can be seen in Fig. 8. Therefore, we can separate their energies, as shown schematically in Fig. 9.

The swell energy E_s can be computed from the spectrum of a coexistent system $\phi(f)$ by

$$E_s = \int_0^{f_1} \phi(f) df, \tag{7}$$

and the wind wave energy E_w can be computed similarly by

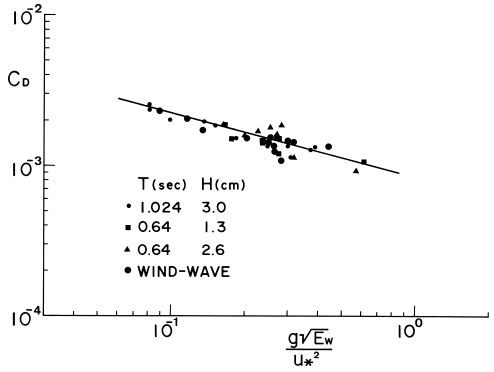

Fig. 10. Plot of the drag coefficient C_D versus dimensionless wind wave energy $g\sqrt{E_w}/u_*^2$.

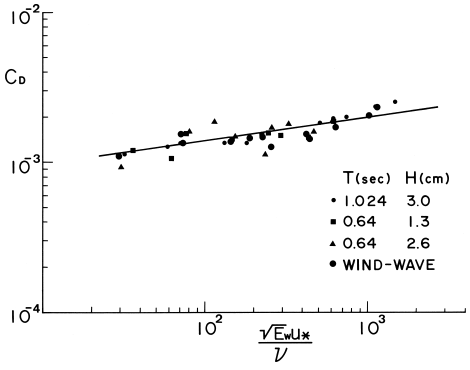

Fig. 11. Plot of the drag coefficient C_D versus Reynolds number $\sqrt{E_w}\,u_*/\nu$.

$$E_w = \int_{f_1}^{f_2} \phi(f)df. \tag{8}$$

After visual inspection of the spectra of the coexistent system, characteristic frequencies f_1 and f_2 were determined respectively as f_1 = 1.8 Hz and f_2 = 40 Hz.

3.3 The dependence of sea surface roughness on wind waves

In order to clarify the dependence of the water surface roughness on wind waves we correlated the drag coefficient C_D with two different wave-dependent parameters, the dimensionless wind wave energy $g\sqrt{E_w}/u_*^2$ and the wave Reynolds number $\sqrt{E_w}\,u_*/\nu$. Here g is the acceleration of gravity, E_w is the energy of wind waves coexisting with opposing swell, which is determined from Eq. (8), and ν is the kinematical viscosity of the air. The results are shown in Figs. 10 and 11. We can see from these figures that the fetch-dependent scatter of the data shown in Fig. 4 decreased considerably in Figs. 10 and 11, though some scattering of the data still remains. The best-fit curves for the data are given by

$$C_D = 8.45\times10^{-4}\left(g\sqrt{E_w}/u_*^2\right)^{-0.407}, \tag{9}$$

$$C_D = 6.20\times10^{-3}\left(\sqrt{E_w}u_*/\nu\right)^{0.169}. \tag{10}$$

Based on the hypothesis of the local equilibrium of winds and wind waves, Masuda and Kusaba (1987) and Kusaba and Masuda (1988) conducted interesting studies on sea surface roughness. They introduced an important dimensionless parameter that controls the sea surface roughness, a wind-wave parameter defined by $u_*\omega_p/g$ $(=2\pi u_* f_m/g)$, where ω_p is the angular frequency of a spectral peak. The wind-wave parameter corresponds to a dimensionless spectral peak frequency. If local equilibrium is satisfied, the wind-wave parameter $u_*\omega_p/g$ $(=2\pi u_* f_m/g)$ is equivalent to the dimensionless wind wave energy $g\sqrt{E_w}/u_*^2$, which is used in Eq. (9). The present data therefore support approximately the idea proposed by Masuda and Kusaba (1987). However, it is important to realize that E_w in Eqs. (9) and (10) includes the energy of wind waves coexisting with and affected by opposing swell, as well as the energy of pure wind waves.

3.4 Attenuation of swell by opposing wind

The attenuation of swell is caused not only by the effect of opposing wind but also by the viscous effect of the water. Therefore, the attenuation of the swell energy E can be written as

$$E = E_0 \exp\left[-(\alpha+\alpha_0)x/\lambda\right], \tag{11}$$

where E_0 is an initial swell energy, E is the swell energy at a propagation distance x, α is an exponential decay rate due to opposing wind and α_0 is an exponential decay rate due to water viscosity. Attenuation of swell energy due to water viscosity can be written as

$$(E)_0 = (E_0)_0 \exp\left[-\alpha_0 x/\lambda\right], \tag{12}$$

where $(E)_0$ is the swell energy at the propagation distance x without wind action and $(E_0)_0$ is the initial swell energy without wind action. From Eqs. (11) and (12) we can get the following relation by dividing Eq. (11) with Eq. (12) and putting $E_0 = (E_0)_0$

$$E/(E)_0 = \left[E_0/(E_0)_0\right]\exp\left[-\alpha x/\lambda\right] = \exp\left[-\alpha x/\lambda\right]. \tag{13}$$

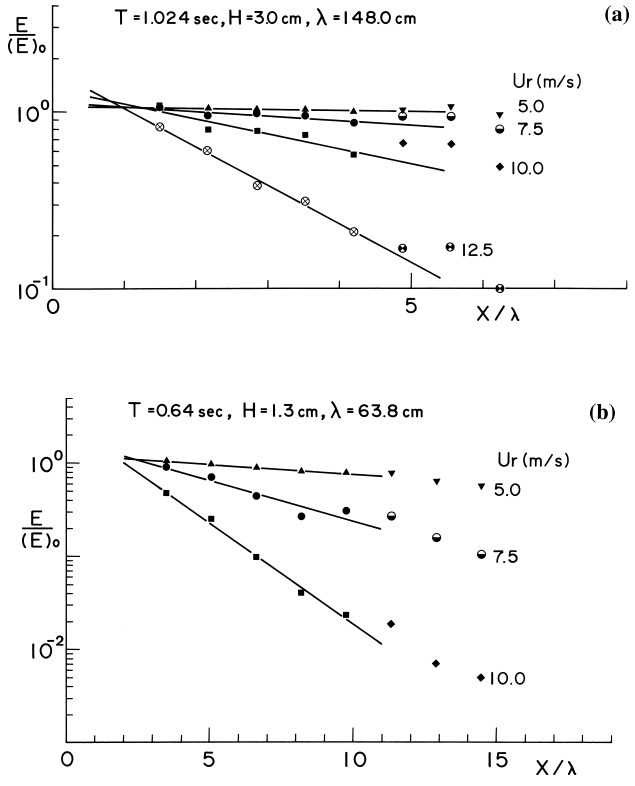

Fig. 12. Plot of swell energy $E/(E)_0$ versus propagation distance x/λ. (a) Swell: T = 1.024 sec, H = 3.0 cm. (b) Swell: T = 0.64 sec, H = 1.3 cm.

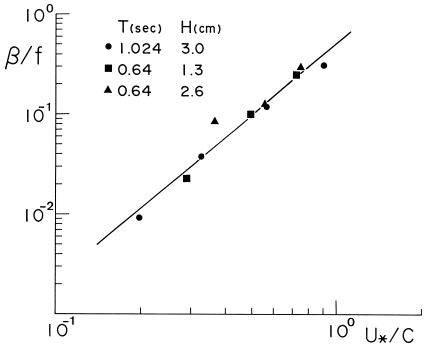

Fig. 13. Plot of the attenuation rate β/f versus wind speed u_*/C.

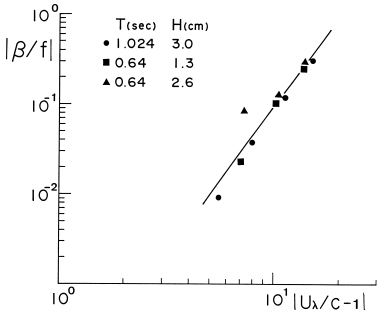

Fig. 14. Plot of the attenuation rate β/f versus wind speed $|(U_\lambda/C) - 1|$.

Normalized swell energy $E/(E)_0$ was plotted against x/λ to determine the exponential decay rate α due to opposing wind. Some examples of the results are shown in Figs. 12(a) and (b). As shown in these figures, the data follow Eq. (13) very well, except for a region of large x/λ values, where the friction velocity of the wind is a little lower than the other area due to the gap between the transition plate and the water surface. By fitting Eq. (13) to the measured data, the exponential decay rate α was determined, where three data for the large values of x/λ were eliminated in the curve fitting for the reason mentioned above. Further, by using a relation $x = C_g t$, the spatial decay rate α was converted to a temporal decay rate β as

$$\beta = \alpha C_g/\lambda. \tag{14}$$

We correlated a dimensionless decay rate β/f with typical dimensionless wind speeds u_*/C and $|(U_\lambda/C) - 1|$ as shown in Figs. 13 and 14, and obtained the following relations,

$$\beta / f = 0.52\left(u_* / C\right)^{2.37}, \tag{15}$$

$$\frac{\beta}{f} = 4.6\times10^{-5}\left|\frac{U_\lambda}{C} - 1\right|^{3.3}, \tag{16}$$

where U_λ is the wind speed at the height of one wave length λ.

Several studies have been published on the attenuation of surface waves by opposing wind. Al-Zanaidi and Hui (1984) reported a theoretical study on the airflow over a wavy surface using a two-equation closure model for the boundary layer turbulence, and determined the growth rate due to following wind and the decay rate due to opposing wind. Their computed decay rate is given by

$$\frac{\beta}{\omega} = A\frac{\rho_a}{\rho_w}\left|\frac{U_\lambda}{C} - 1\right|^2, \tag{17}$$

where ρ_w is water density and the constant A is given by

A = 0.024 for smooth or transitional surface,

A = 0.040 for rough surface.

By putting $A = 0.04$ and $\rho_a/\rho_w = 1.2 \times 10^{-3}$ and using frequency f instead of the angular frequency ω, Eq. (17) becomes

$$\frac{\beta}{f} = 3.0 \times 10^{-4} \left| \frac{U_\lambda}{C} - 1 \right|^2 . \tag{18}$$

They also used the same theoretical model to compute the growth rate of water waves due to a following wind, which was about 1.5 times greater than the decay rate.

Recently Donelan (1999) reported an interesting study on the wind-induced growth and attenuation of laboratory waves. He measured the direct energy input to pure wind waves, and that to the coexistent system of wind waves and following (or opposing) swell, respectively, by computing the fractional energy input to each wave from the data of the quadrature spectrum between air-pressure and water-surface elevation. It should be noted that the swell used in his experiment is not monochromatic waves but has the spectral form of a JONSWAP type. The wind-induced attenuation rate of the swell by opposing wind is given, after slight modification, by

$$\frac{\beta}{f} = 8.3 \times 10^{-4} \left| \frac{U_{\lambda/2}}{C} - 1 \right|^2 , \tag{19}$$

where $U_{\lambda/2}$ is the wind speed at the height of a half wave length $\lambda/2$ and C corresponds to the phase speed of the wave component at spectral peek frequency. In order to compare Eq. (19) with Eqs. (16) and (18), Eq. (19) is converted to the following form, where U_λ is used as a representative wind speed

$$\frac{\beta}{f} = 6.9 \times 10^{-4} \left| \frac{U_\lambda}{C} - 1 \right|^2 . \tag{20}$$

The conversion was done simply by dividing the front constant in Eq. (19) by 1.2 in reference to the study of Mitsuyasu and Kusaba (1988). In their study, the wind-induced growth rate of laboratory waves was measured and the growth rate was correlated with various representative wind speeds, such as u_*, U_λ , $U_{\lambda/2}$ and U_{10} . The ratio of the constant in the form for $U_{\lambda/2}$ and that for U_λ gives approximately 1.2 (see Appendix).

Quite recently, Peirson *et al*. (2003) measured the attenuation of mechanically generated waves due to an opposing wind. They used almost the same technique as ours; they directly measured the attenuation of mechanically generated monochromatic waves due to an opposing wind. They obtained the following relations

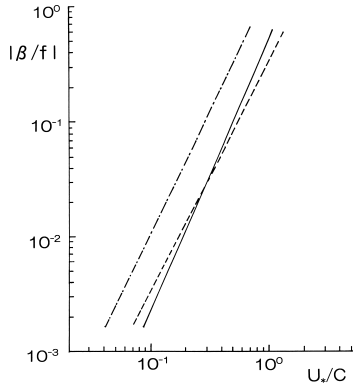

Fig. 15. Various relations for the growth and decay of swell by wind. —: Eq. (15), –·–·–: Eq. (24), - - -: Eq. (26).

$$\frac{\beta}{f} = 2.36 \times 10^{-4} (ak)^{0.240} \left| \frac{U_{\lambda/2}}{C} - 1 \right|^{3.265} , \tag{21}$$

$$\beta / f = 2.275 (ak)^{0.238} \left(u_* / C \right)^{2.112} . \tag{22}$$

Both of these relations for attenuation rate of swell contain a new parameter, swell steepness ak ($=\pi H/\lambda$), where a ($=H/2$) is an amplitude of swell and k ($=2\pi/\lambda$) is the wave number. Since the dependence of the attenuation rate on the wave steepness ak is relatively weak in their forms, we tentatively use the initial steepness $ak_0 = 0.125$ in their relations instead of ak. Then Eqs. (21) and (22) reduce respectively to

$$\frac{\beta}{f} = 1.43 \times 10^{-4} \left| \frac{U_{\lambda/2}}{C} - 1 \right|^{3.265} , \tag{23}$$

$$\beta / f = 1.39 \left(u_* / C \right)^{2.112} . \tag{24}$$

Furthermore, in order to compare Eq. (23) with the other relations, Eq. (23) was changed to the following form as a function of U_λ instead of $U_{\lambda/2}$ by simply dividing the front constant in Eq. (23) by 1.2, for the reason mentioned previously,

$$\frac{\beta}{f} = 1.19 \times 10^{-4} \left| \frac{U_\lambda}{C} - 1 \right|^{3.265} . \tag{25}$$

Figure 15 shows our present relation Eq. (15) and a modified form of the relation of Peirson *et al*. (2003) Eq. (24), where the friction velocity of the wind, u_* is used as a reference wind speed. As a reference, the relation for the growth rate of water waves due to a following wind

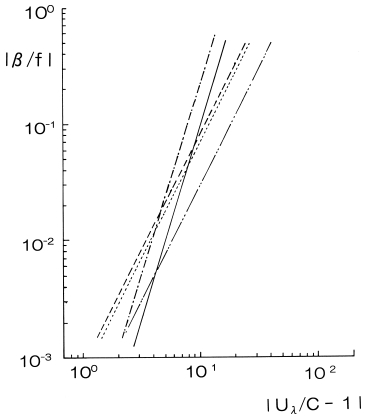

Fig. 16. Various relations for the decay of swell by opposing wind. —: Eq. (16), ·····: Eq. (20), –·–·–: Eq. (25), –··–··–: Eq. (18), - - -: Eq. (27).

(Mitsuyasu and Honda, 1982)

$$\beta / f = 0.34\left(u_* / C\right)^2 \tag{26}$$

is included in the figure. This relation was obtained in the same wind wave flume by using a similar technique as the one reported here.

It is interesting that the present relation for the decay rate of water waves due to opposing wind is, in a range $0.1 < u_*/C < 1.0$, quite similar to the relation for the growth rate of water waves due to following wind, except for the sign. This is different from the results reported by Al-Zanaidi and Hui (1984) and Donelan (1999), which show much a larger growth rate than decay rate. With regard to the results of Al-Zanaidi and Hui (1984), since they made several assumptions on the boundary layer over the wave surface in their theoretical computations, there may be a possibility that their assumptions are different from our experimental conditions. Furthermore, the values of the decay rate and the growth rate themselves are slightly different from ours. The modified form Eq. (24) of the relation Eq. (22) obtained by Peirson *et al*. (2003) gives much larger values, about 3.5 times larger than those given by the present one, Eq. (15).

Figure 16 shows our present relation Eq. (16), a modified form Eq. (20) of the relation Eq. (19) of Donelan (1999), and the modified form Eq. (25) of the relation Eq. (21) of Peirson *et al*. (2003). As references, Fig. 16 includes the relation Eq. (18) of Al-Zanaidi and Hui (1984) and the following relation for the growth rate of water waves by following wind (Mitsuyasu and Kusaba, 1988),

$$\frac{\beta}{f} = 8.2 \times 10^{-4} \left| \frac{U_\lambda}{C} - 1 \right|^2 . \tag{27}$$

This relation was also obtained in the same wind wave flume by using a similar technique as the present one.

Note that absolute values are shown in Figs. 15 and 16; the relations for the decay rate and that for the growth rate are shown in the same coordinate. Figure 16 shows that the relation Eq. (25) of Peirson *et al*. (2003) gives the largest values among these relations and it gives about double the value that our present relation Eq. (16) gives. The relation obtained by Donelan (1999) Eq. (20) is almost the same as the relation Eq. (27) for the growth rate of water waves due to a following wind (Mitsuyasu and Kusaba, 1988). The relation Eq. (18) of Al-Zanaidi and Hui (1984) gives the smallest value among these relations and it gives a value one order of magnitude smaller than that given by the relation of Peirson *et al*. (2003).

It is an unexpected result that the relation of Peirson *et al*. (2003) gives about twice (in the expression using U_λ) or 3.5 times (in the expression using u_*) greater values than those of our present relations. They used experimental conditions which are quite similar to those of Mitsuyasu and Honda (1982), except for the wind direction; the frequency of paddle waves, their wave steepness and wind speeds used in their experiment are almost the same as those given in Mitsuyasu and Honda (1982). Furthermore, they used the same technique as ours for the determination of decay rate of waves due to an opposing wind. Our present experiment was performed in the same wind wave flume as used by Mitsuyasu and Honda (1982) and the experimental conditions are quite similar to those in their study, except for the wind direction.

One of the sources of uncertainty in these results is the friction velocity of the wind. The friction velocity of the wind in the flume is not only difficult to determine but also not uniform along the wind wave flume. Due to the boundary condition of the tank and also the change of water surface condition along the flume, the friction velocity changes slightly along the flume. We used averaged values of the friction velocities measured at three stations along the tank, while Peirson *et al*. (2003) used the value at one station near the center of the test section. However, such an uncertainty will introduce differences in the results of at most some ten percent.

One of the large differences in these two experiments is a different scale of the wind wave flume. We used a wind wave flume 0.8 m high (water depth 0.35 m), 0.6 m wide and with a test section about 15 m long, while they used a wind wave flume 1.55 m high (water depth 1.1 m), 0.9 m wide and with a test section about 10 m. Although the air gap of their tank is the same as ours, the width of their tank is 1.5 times wider than ours and the water depth in their tank is about three times deeper than ours.

Recently Mizuno (2003) reported a fundamental

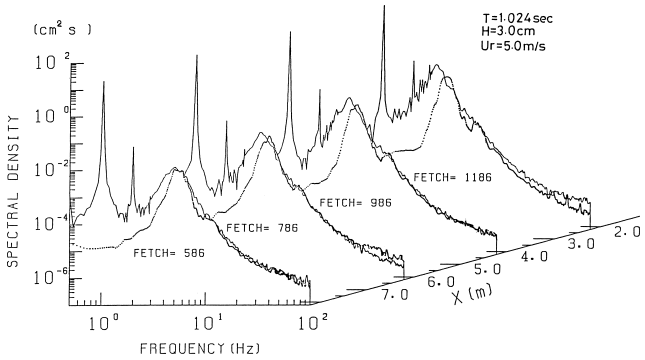

Fig. 17. Spectra of coexistent system of wind waves and swell. Swell: T = 1.024 sec, H = 3.0 cm, wind speed Ur = 5.0 m/s.

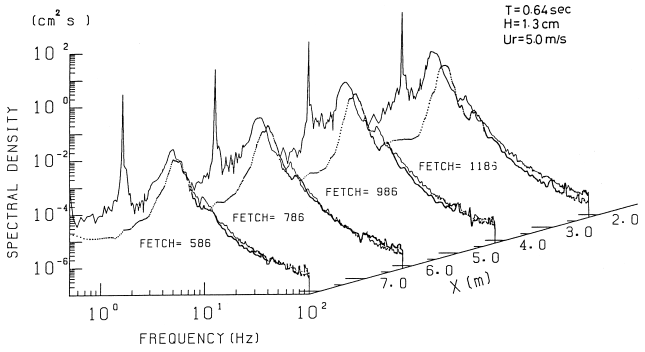

Fig. 18. Spectra of coexistent system of wind waves and swell. Swell: T = 0.64 sec, H = 1.3 cm, wind speed Ur = 5.0 m/s.

study on the effect of swell on wind-induced current. He found the following very interesting phenomena.

1) In addition to a primary flow (dominant drift current and its return flow), wind generates a secondary flow (downward flow near both side walls of the flume, upward flow near the center line of the flume).

2) These flow structures are considerably affected by swell; a following swell strengthens the secondary flow and weakens the primary flow, while an opposing swell weakens the secondary flow and strengthens the primary flow. The latter phenomenon was also found by Cheng and Mitsuyasu (1992).

Although Mizuno (2003) was mainly concerned with the effect of swell on the wind-induced current system in the flume, the swell will also be affected by the flow structure. If the interaction between the swell and wind-induced current is one of the important factors for the attenuation of swell by opposing wind, as suggested by Peirson *et al*. (2003), the difference in the flume (particularly its aspect ratio) will introduces some difference in the attenuation rate of swell, because the secondary flow usually depends on the aspect ratio of the tank (on the water side): it is weak for large aspect ratio (wide tank) and strong for small aspect ratio (narrow tank). The aspect ratio of the tank used by Peirson *et al*. (2003) is 0.82 and that of our tank is 1.7, i.e., it is about twice as large.

However, for more detailed discussions we need more fundamental data, both on the wind induced current system in the flume and on the interaction between swell and the current system. Furthermore, if the wind-induced current plays an important role in the phenomena, there may be a possibility that the phenomena observed in the ocean are slightly different from those in a laboratory flume, because the wind-induced current in a laboratory flume is affected, to some extent, by boundary conditions and it will be slightly different from the wind-induced current in the ocean.

3.5 Effect of opposing swell on the growth of wind waves

Attenuation of wind waves by a following steep swell was discovered many years ago (Mitsuyasu, 1966; Phillips and Banner, 1974). This phenomenon has been confirmed later in many studies (e.g., Hatori *et al*., 1981; Donelan, 1987, 1999; Sakai *et al*., 1994), though the attenuation mechanism is still controversial.

In contrast to many studies on the effect of following swell on wind waves, there have been few studies on the effect of opposing swell. Dobson *et al*. (1988) analyzed their field data of ocean waves and reported that an opposing swell does not influence the growth of fetch-limited wind waves. Recently, Hanson and Phillips (1999) investigated wind sea growth and dissipation in a swell-dominated open ocean environment. They obtained a similar result; dimensionless wind sea energy is scaled with inverse wave age, independently of swell.

Typical examples of our measured frequency spectra of co-existent systems of wind waves and opposing swell are shown in Fig. 17, where the spectra of pure wind wave unaffected by the swell (dotted curves) are superimposed for comparison. These figures show four spectra measured at four different fetches, though the spectra were actually measured at eight different fetches. Figure 18 shows similar spectra of a co-existent system for different swell of short period. In each spectrum a sharp spike in the low-frequency side corresponds to the swell spectrum and a gentle peak in the high-frequency side corresponds to the wind wave spectrum. Figure 17 shows a secondary spike that corresponds to a secondary harmonic of the swell spectrum, while it cannot be seen in Fig. 18. In the latter case, the secondary harmonics might submerge into the wind wave spectrum.

One of the most interesting things in the spectra shown in Figs. 17 and 18 is the increase of the spectral energy of wind waves coexisting with opposing swell as compared to those without swell. Furthermore, the spectral peak of the wind waves is shifted to the low-frequency

side. That is, an opposing swell intensifies the growth of wind waves, while a following swell suppresses the growth of wind waves, as reported in many previous studies. In order to examine the effect of opposing swell on wind waves quantitatively, the energy of wind waves coexisting with opposing swell is normalized by the energy of wind waves without swell and plotted against the steepness of the swell under wind action, H_1/λ. Here the swell height H_1 under wind action was determine from the swell energy E_s using the relation

$$H_1 = \left(8E_s\right)^{1/2}. \tag{28}$$

The results are shown in Fig. 19, where our previous result for the following swell (Mitsuyasu, 1966) is also shown at the lower side of each figure for comparison. Since the data scatters considerably, sectional mean values of $E_w/(E_w)_0$ were plotted in the lower figure. As can be seen from Fig. 19, an opposing swell displays a quite different effect on wind waves; it intensifies the growth of wind waves, while the following swell attenuates wind waves. This is quit different from the prediction of the theory of Phillips and Banner (1974), which predicts the attenuation of wind waves by swell irrespective of its direction, though the attenuation rate is slightly different. We tried to apply the model of Chen and Belcher (2000), but were unsuccessful. Further studies are needed to clarify this problem.

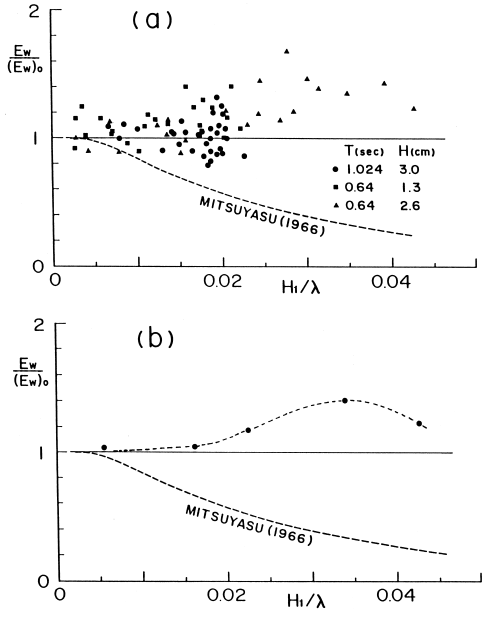

Fig. 19. Effect of swell steepness on the growth of wind waves. (a): Original data, (b): sectional mean values. Each figure include the result for the case of following wind (Mitsuyasu, 1966).

3.6 *Effect of opposing swell on the high frequency spectrum of wind waves*

High frequency components of wind waves are important not only for air-sea interactions but also for microwave remote sensing of the sea surface. For example, the wind-speed dependence of the high-frequency components of wind waves is used to measure sea surface wind with a microwave scatterometer. Figure 20 shows the wind-speed dependence of the spectrum of wind waves coexisting with opposing swell. The spectra shown in the left figure were measured at the fetch F = 5.86 m and those in the right figure were measured at fetch F = 9.86 m, both for wind speeds Ur = 5.0, 7.5, 10.0 and 12.5

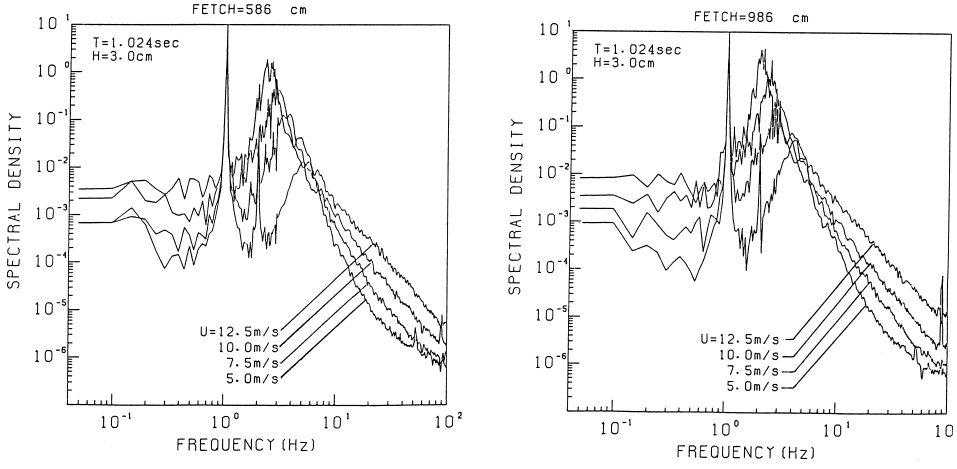

Fig. 20. Growth of high frequency spectra of wind waves coexisting with swell. Swell: T = 1.024 sec, H = 3.0 cm. Left figure: F = 5.86 m, right figure: F = 9.86 m.

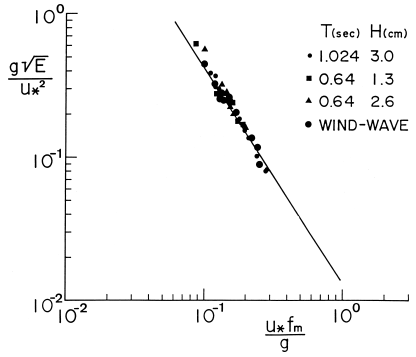

Fig. 21. Plot of dimensionless wind wave energy $g\sqrt{E_w}/u_*^2$ versus dimensionless spectral peek frequency $u_* f_m/g$. —: Eq. (29).

(m/sec). We can see the usual systematic increase of the high frequency spectrum of wind waves with increasing wind speed. However, we need to confirm whether or not such a property is the same as that without opposing swell. As for the effects of following swell, Mitsuyasu (1997) found that the effect is negligibly small.

For this purpose we look back Figs. 17 and 18, shown previously. We can see that the high frequency part of the wind wave spectrum is not much affected by opposing swell either. However, closer examination of the figures shows a small increase of the spectral energy in a high frequency region. This can be attributed to the small increase of wind shear stress by opposing swell, which has been discussed in Subsection 3.1.

3.7 Local equilibrium of winds and wind waves coexisting with opposing swell

The increase of wind shear stress by opposing swell and the increases of the spectral energy, not only in a dominant frequency region but also in a high-frequency region of the wind wave spectrum, suggest the local equilibrium of winds and wind waves coexisting with opposing swell. Toba (1972) proposed the "three-second power law" based on the hypothesis of the local equilibrium of winds and wind waves. In order to confirm this, we plotted the dimensionless wind wave energy $g\sqrt{E_w}/u_*^2$ against the dimensionless spectral peak frequency $u_* f_m/g$ in Fig. 21. The solid line in the figure shows a form of the "three-second power law" derived from our previous data of pure wind wave spectra (Mitsuyasu, 1968)

$$g\sqrt{E_w}/u_*^2 = 1.3\times10^{-2}\left(u_* f_m / g\right)^{-3/2}. \qquad (29)$$

As shown in the figure, wind waves coexisting with opposing swell satisfy the hypothesis of local equilibrium and the "three-second power law". The result also supports the finding of the field observation by Hanson and Phillips (1999), that dimensionless wind wave energy is found to scale with inverse wave age independently of swell.

Sakai *et al.* (1994) reported a similar study on the local equilibrium of winds and wind waves coexisting with a following swell. They plotted the dimensionless wind wave energy and the dimensionless spectral peak frequency respectively against a dimensionless fetch. The relation between the dimensionless spectral peak frequency of wind waves and the dimensionless fetch is unaffected by the following swell. However, the dimensionless wind wave energy coexisting with a following swell depends not only on the dimensionless fetch but also on the steepness of the swell. A universal form for the local equilibrium of winds and wind waves can therefore not be obtained for wind waves coexisting with a following swell.

4. Application to Oceanographic Phenomena

As far as pure wind waves are concerned, dynamical similarity is satisfied approximately both for laboratory wind waves and for wind waves in the ocean (e.g., Mitsuyasu, 1968; Hasselman *et al.*, 1973; Donelan *et al.*, 1985). That is, wind waves follow almost the same fetch relations or satisfy the same "three-second power law" (Toba, 1972). As for wind waves coexisting with swell, most of the wave observations in the ocean show little effect of swell on wind waves (Dobson *et al.*, 1988; Hanson and Phillips, 1999), the dominant reason being that, in many cases, the steepness of swell is very small in the ocean. This is partly due to the fact that the swell has from a far distant origin and further, its growth rate is very small, even in a following wind area because of its small inverse wave age, as mentioned by Chen and Belcher (2000). As shown previously in Fig. 19, the effect of swell of small steepness, says $H/\lambda < 0.01$, is very small for wind waves regardless of the swell direction. This fact must be borne in mind, because in many laboratory experiments we usually use swell of relatively large steepness in order to give it a prominent effect.

Furthermore, for the case of opposing swell, the present study shows that the swell intensifies both wind shear stress and wind wave energy and does not disturb the local similarity of wind and wind waves. This provides an explanation for the result of Hanson and Phillips (1999), that dimensionless wind wave energy is scaled with inverse wave age independently of swell. However, this is not the case for following swell. As clearly shown by Sakai *et al.* (1994) dimensionless wind wave energy decreases with the increase of swell steepness, while dimensionless spectral peak frequency, which corresponds to the inverse wave age, is not affected by the following swell. Therefore, dimensionless wind wave energy can-

not be scaled universally with the inverse wave age as far as laboratory wind waves and following swell are concerned. However, if the swell steepness is small, its effect on wind waves will be small too, as mentioned above.

5. Conclusions

The magnitude of the attenuation rate of swell by an opposing wind is almost the same as that of the growth rate of swell caused by a following wind, except for its negative sign. This is different from the results of Al-Zanaidi and Hui (1984) and Donelan (1999); their results give a greater magnitude of the growth rate of swell due to a following wind than that of the attenuation rate of swell by an opposing wind. The attenuation rate reported here is much smaller than that observed recently by Peirson *et al*. (2003), though the reason is not clear. The difference in the scale of wind-wave tank and associated difference of current structure may provide some explanation, but this problem is left for future studies.

Wind wave energy tends to increase with the increase of the steepness of opposing swell. This trend is very different from that shown by a following swell; as usually observed, wind wave energy decreases with increasing the steepness of following swell. The phenomenon is very different from the prediction of the model of Phillips and Banner (1974). Further studies are needed to clarify the problem. Opposing swell also increases wind shear stress and accordingly the drag coefficient of the water surface increases. The drag coefficient of the water surface is well correlated with dimensionless wind wave energy and Reynolds number, even when the opposing swell coexists.

A more important point is that the local equilibrium of winds and wind waves is satisfied, even when wind waves coexist with opposing swell. In association with relatively small steepness of swell in the ocean, this provides an explanation for the result of Hanson and Phillips (1999), that dimensionless wind wave energy in the ocean is scaled with inverse wave age independently of swell. However, the local equilibrium is not satisfied for wind waves coexisting with a following swell.

Spectral energy in a high-frequency region of wind wave spectrum increases slightly due to the effect of opposing swell. This is consistent with the increase of wind shear stress by opposing swell, because the high-frequency spectrum of wind waves depends on the wind shear stress (e.g., Mitsuyasu and Honda, 1974). In the case of a following swell, however, spectral energy in a high-frequency region of the wind wave spectrum is not affected by the swell, even when the spectral energy in a dominant frequency region is greatly suppressed (Mitsuyasu, 1997). Since the measured wind shear stress is not much affected by the following swell (Mitsuyasu and Maeda, 2002), the result seems to be consistent.

Acknowledgements

We wish to express our thanks to Professor A. Masuda of Kyushu University for his constant and fruitful discussions of the problem. We also express our gratitude to two reviewers for their valuable comments.

Appendix

Mitsuyasu and Kusaba (1988) studied the relation between the wind-induced growth rate of water waves and various characteristic wind speeds over a water surface. They correlated the measured growth rate β with the characteristic wind speeds u_*, $U_{\lambda/2}$, U_λ and U_{10}, where u_* is the friction velocity of the wind, and $U_{\lambda/2}$, U_λ and U_{10} are the wind speeds at the heights of $\lambda/2$, λ and 10 m above water surface (λ: wave length), respectively. Important results are summarized as follows.

1) Within a range of a dimensionless wind speed, $0.1 < u_*/C < 0.6$, empirical relations between the wind-induced growth rate and the characteristic wind speeds are given respectively by

$$\beta/f = 0.33\ (u_*/C)^2, \tag{A1}$$

$$\beta/f = 9.8 \times 10^{-4}\ (U_{\lambda/2}/C - 1)^2, \tag{A2}$$

$$\beta/f = 8.2 \times 10^{-4}\ (U_\lambda/C - 1)^2, \tag{A3}$$

$$\beta/f = 4.7 \times 10^{-4}\ (U_{10}/C - 1)^2, \tag{A4}$$

where f and C are frequency and phase velocity of the water waves respectively.

2) The correlation coefficients in these relations are in a range, 0.90~0.92, and there are no appreciable differences in the correlation coefficients.

3) Equation (A3) has a similar form to the theoretical relation derived by Al-Zanaidi and Hui (1984), but the present relation gives larger value of the growth rate (by a factor of about 1.7) than that given by their relation.

From Eqs. (A2) and (A3) we can get an approximate conversion coefficient 1.2 to change the relation for U_λ to the relation for $U_{\lambda/2}$.

On the other hand, the definitions of $U_{\lambda/2}$ and U_λ give the following equations,

$$U_\lambda = \frac{u_*}{\kappa} \ln \frac{\lambda}{z_0}, \tag{A5}$$

$$U_{\lambda/2} = \frac{u_*}{\kappa} \ln \frac{\lambda}{2z_0}. \tag{A6}$$

From Eqs. (A5) and (A6) we can get

$$\frac{U_\lambda}{U_{\lambda/2}} = \frac{\ln \lambda / z_0}{\ln \lambda / z_0 - \ln 2} = \frac{1}{1 - \ln 2 / \left(\ln \lambda / z_0\right)} = \frac{1}{1 - 0.69 / \left(\ln \lambda / z_0\right)}. \quad \text{(A7)}$$

In our laboratory conditions λ is of the order of 10^2 cm and z_0 is of the order of 10^{-2} cm. Therefore, $\ln\lambda/z_0$ becomes approximately 9.2 and Eq. (A7) gives roughly $U_{\lambda/2} = 1.08\ U_\lambda$ and $(U_{\lambda/2})^2 = 1.17\ (U_\lambda)^2$. In this way we can get the conversion coefficient of approximately 1.17. This is nearly equal to the conversion coefficient 1.2 obtained in our study mentioned above. If the wind-induced growth rate of waves is proportional to the third power of the characteristic wind speed, the conversion coefficient becomes approximately 1.26.

References

Al-Zanaidi, M. A. and W. H. Hui (1984): Turbulent airflow over water waves—a numerical study—. *J. Fluid Mech.*, **148**, 225–246.

Chen, G. and S. E. Belcher (2000): Effect of long waves on wind-generated waves. *J. Phys. Oceanogr.*, **30**, 2246–2256.

Cheng, Z. and H. Mitsuyasu (1992): Laboratory study of surface drift current induced by wind and waves. *J. Fluid Mech.*, **243**, 247–259.

Dobson, F., W. Perie and B. Toulany (1988): On the deep-water fetch law for wind-generated surface gravity waves. *Atmos.-Ocean*, **27**(1), 210–236.

Donelan, M. A. (1987): The effect of swell on the growth of wind waves. *Johns Hopkins APL, Tech. Dig.*, **8**, 18–23.

Donelan, M. A. (1999): Wind-induced growth and attenuation of laboratory waves. p. 183–194. In *Wind-over-Wave Coupling*, ed. by S. G. Sajjadi, N. H. Thomas and J. C. R. Hunt, Clarendon Press, Oxford

Donelan, M. A., J. Hamilton and W. H. Hui (1985): Directional spectra of wind-generated waves. *Phil. Trans. Roy. Soc. London*, (A) **315**, 509–562.

Hanson, J. L. and O. M. Phillips (1999): Wind sea growth and dissipation in open ocean. *J. Phys. Oceanogr.*, **29**, 1633–1648.

Hasselmann, K. and 15 authors (1973): Measurements of wind-wave growth and swell decay during the Joint North Sea Wave Project (JONSWAP). *Dt. Hydrogr. Z.*, **A8**(12), 95 pp.

Hatori, M. M., Y. Tokuda and Y. Toba (1981): Experimental studies on strong interactions between regular waves and wind waves-1. *J. Oceanogr. Soc. Japan*, **37**, 111–119.

Kusaba, T. and A. Masuda (1988): The roughness height and drag law over the water surface based on the hypothesis of local equilibrium. *J. Oceanogr. Soc. Japan*, **45**, 200–212.

Masson, D. (1993): On the nonlinear coupling between swell and wind waves. *J. Phys. Oceanogr.*, **23**, 1249–1258.

Masuda, A. and T. Kusaba (1987): On the local equilibrium of winds and wind-waves in relation to surface drag. *J. Oceanogr. Soc. Japan*, **43**, 28–36.

Mitsuyasu, H. (1966): Interaction between water wave and wind (I). *Rep. Res. Inst. Appl. Mech., Kyushu Univ.*, **14**, 67–88.

Mitsuyasu, H. (1968): On the growth of the spectrum of wind-generated waves 1. *Rep. Res. Inst. Appl. Mech., Kyushu Univ.*, **16**, 459–465.

Mitsuyasu, H. (1992): Wave breaking in the presence of wind drift and opposed swell. p. 147–153. In *Breaking Waves*, ed. by M. L. Banner and R. H. J. Grimshaw, Springer Verlag.

Mitsuyasu, H. (1997): On the contribution of swell to sea surface phenomena. *Transaction of the ISOPE*, **7**, 241–245.

Mitsuyasu, H. and T. Honda (1974): The high frequency spectrum of wind-generated waves. *J. Oceanogr. Soc. Japan*, **30**, 185–198.

Mitsuyasu, H. and T. Honda (1982): Wind-induced growth of water waves. *J. Fluid Mech.*, **123**, 425–442.

Mitsuyasu, H. and T. Kusaba (1984): Drag coefficient over water surface under the action of strong wind. *Natural Disaster Science*, **6**, 43–50.

Mitsuyasu, H. and T. Kusaba (1988): On the relation between the growth rate and wind speed. *J. Oceanogr. Soc. Japan*, **44**, 136–142.

Mitsuyasu, H. and Y. Maeda (2002): On the contribution of swell to sea surface phenomena (2). *Transaction of the ISOPE*, **12**, 237–242.

Mitsuyasu, H. and Y. Yoshida (1989): Air-sea interactions under the existence of swell propagating against the wind. *Bulletin of the Res. Inst. Appl. Mech., Kyushu Univ.*, No. 68, 47–71 (in Japanese).

Mitsuyasu, H. and Y. Yoshida (1991): The effect of swell on the growth of wind waves. p. 381–391. In *Oceanography of Marginal Seas*, ed. by K. Takano, Elsevier.

Mizuno, S. (2003): Laboratory experiments on the effects of mechanical waves on the mean and turbulent flow under the wind waves. *Proceedings of 2003 Meeting of Japan Society of Fluid Mechanics*, 41–42.

Peirson, W. L., A. W. Garcia and S. E. Pells (2003): Water wave attenuation due to wind. *J. Fluid Mech.*, **487**, 345–365.

Phillips, O. M. and M. L. Banner (1974): Wave breaking in the presence of wind drift and swell. *J. Fluid Mech.*, **66**, 625–640.

Sakai, J., T. Kusaba and A. Masuda (1994): An experimental study on the interaction between swells and wind waves. *Bulletin of the Res. Inst. Appl. Mech., Kyushu Univ.*, No. 76, 123–142 (in Japanese).

Toba, Y. (1972): Local balance in the air-sea boundary process 1—on the growth process of wind waves—. *J. Oceanogr. Soc. Japan*, **28**, 109–121.

Tsuruya, H. (1988): Experimental study on the wave decay in an opposing wind. *Coastal Engineering in Japan*, **30**, 25–43.

Wright, J. W. (1976): Wind drift and wave breaking. *J. Phys. Oceanogr.*, **6**, 402–405.